Polarization dynamics of Bragg solitons

Alexey V. Yulin and Dmitry V. Skryabin
Department of Physics, University of Bath, Bath BA2 7AY, United Kingdom

William J. Firth
Department of Physics and Applied Physics, University of Strathclyde, Glasgow G4 0NG, United Kingdom

(Received 21 March 2002; published 9 October 2002)

The families of vectorial Bragg solitons existing in transversely periodic media and their stability properties are studied in detail. Two qualitatively distinct types of polarization instabilities have been found. One leads to the significant radiation transfer into nonsolitonic forms, while the other mainly redistributes energy between two soliton components.

DOI: 10.1103/PhysRevE.66.046603 PACS number(s): 42.65.Tg, 42.65.Sf, 42.79.Dj

I. INTRODUCTION

It is known that so-called gap or Bragg solitons can exist in nonlinear media with one-dimensional (1D) periodic modulation of the refractive index, see, e.g., Refs. [1,2]. The physics behind them differs significantly from the nonlinear Schrödinger (NLS) solitons. Bright NLS solitons in self-focusing media can be interpreted as due to the phenomenon of the nonlinearity-induced total internal reflection of light from the periphery of the soliton itself. In the case of periodic media the reflection of light from the periphery towards the soliton center is due to the Bragg effect, which creates a forbidden gap between the ''conduction'' and the ''valence'' bands in the periodic structure, which is often referred as 1D photonic crystal [3]. Bragg solitons exist at frequencies that lie in the gap, but where a nonlinear change of refractive index shifts its boundaries. This shift can be positive or negative, since it does not matter whether the gap is shifted above or below the soliton frequency, so long as the latter is out of the forbidden gap for propagation.

The present paper deals with the properties of vector Bragg solitons in an anisotropic one-dimensional periodic structure. We consider spatial solitons, i.e., a quasi-one-dimensional beam propagating in a planar waveguide with periodic modulation of the refractive index transverse to the propagation axis. This geometry is interesting in allowing bright spatial solitons in media with either focusing or defocusing nonlinearity, so that spatial self-trapping can be observed over a wide frequency range. In contrast to the familiar case of temporal Bragg solitons in the optical fibers, Bragg solitons self-trapped in the direction transverse to the direction of propagation have not been investigated so far.

The paper is organized as following. In the following section, we describe the system and introduce model equations. In Sec.III, we introduce families of the scalar and vectorial Bragg solitons. In the Sec. IV, we study their stability and make comparison with results known for vector NLS [4–7] and scalar Bragg solitons [8–10].

II. MODEL EQUATIONS

Starting from the full set of Maxwell equations describing propagation of electromagnetic waves in an anisotropic planar waveguide with refractive index weakly modulated across the propagation direction (see Fig. 1), we have derived the following reduced system of coupled propagation equations:

$$i\partial_z E_{r,l}+\partial_{xx}E_{r,l}+[\delta/2+f(x)]E_{r,l}+[\alpha|E_{r,l}|^2 +(\alpha+2\beta)|E_{l,r}|^2]E_{r,l}-\delta E_{l,r}/2=0. \quad (1)$$

Here E_r and E_l are envelopes (slowly varying along z) of the right and left circular polarization components of the electric field

$$\vec{E}=(E_x,E_y)^T=\frac{1}{\sqrt{2}}[E_r+E_l,i(E_r-E_l)]^T. \quad (2)$$

Apart from the function $f(x)$ (see below), these equations are similar to the well-known model describing the transverse effects in planar waveguides, see e.g. Refs. [4–6,11]. $\delta=(\epsilon_y-\epsilon_x)/\epsilon_x$ accounts for linear birefringence of the crystal, where $\epsilon_{x,y}$ are space-independent components of the linear dielectric susceptibility tensor taken in the normal coordinates. The nonlinear part of the displacement vector

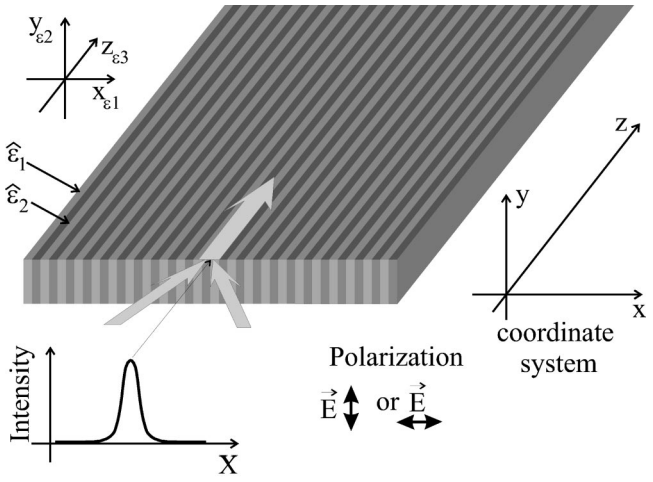

FIG. 1. ■

entering Maxwell equations was taken in the form $\vec{D}=\alpha\epsilon_x|\vec{E}|^2\vec{E}+\beta\epsilon_x(\vec{E}\vec{E})\vec{E}^*$ [12]. α and β describe self- and cross-phase modulation, respectively, due to the nonlinear part of the refractive index [12]. If β is not equal to α, the medium exhibits nonlinear birefringence. $f(x)$ describes a weak spatially dependent contribution to the linear susceptibility, a linear index modulation that creates a forbidden gap for waves propagating in the x direction. The space coordinates x and z are scaled to the wavelength and diffraction length, respectively.

Assuming that the index modulation is weak enough and that the soliton width is much greater than modulation period, we can represent the soliton field as a superposition of two waves, which have oppositely directed x components of their wave vectors. This, in essence, is equivalent to the coupled-mode approach applied in the case of fiber Bragg solitons [2,13]. It is convenient to switch to a linear polarization basis at this stage, so we further transform Eq. (1) reducing them to coupled-mode equations through the substitution

$$E_{x,y}=\frac{1}{\sqrt{\mu}}e^{i(\pi^2/2L^2)z}[E_{x,y}^{(+)}(x,z)e^{i(\pi/L)x} + E_{x,y}^{(-)}(x,z)e^{-i(\pi/L)x}]. \tag{3}$$

Here, $E_{x,y}^{(\pm)}$ are slow functions of x, $\mu=|(1/L)\int_0^L f(x)e^{i(2\pi/L)x}dx|$ is a coupling coefficient, and L is the modulation period. Introducing new variables $\tilde{z}=(1/2)\mu z$ and $\tilde{x}=(L/2\pi)\mu x$ and omitting the tilde in the following, we get the set of four equations

$$i\partial_z E_x^{(\pm)}\pm i\partial_x E_x^{(\pm)}+E_x^{(\mp)}+[(\alpha+\beta)(|E_x^{(\pm)}|^2+2|E_x^{(\mp)}|^2) + \alpha(|E_y^{(\pm)}|^2+|E_y^{(\mp)}|^2)]E_x^{(\pm)}+\alpha E_y^{(\pm)}E_y^{(\mp)*}E_x^{(\mp)} + \beta E_y^{(\pm)2}E_x^{(\pm)*}+2\beta E_y^{(\pm)}E_y^{(\mp)}E_x^{(\mp)*}=0, \tag{4}$$

$$i\partial_z E_y^{(\pm)}\pm i\partial_x E_y^{(\pm)}+E_y^{(\mp)}+\delta E_y^{(\pm)}+[(\alpha+\beta)(|E_y^{(\pm)}|^2 + 2|E_y^{(\mp)}|^2)+\alpha(|E_x^{(\pm)}|^2+|E_x^{(\mp)}|^2)]E_y^{(\pm)} + \alpha E_x^{(\pm)}E_x^{(\mp)*}E_y^{(\mp)}+\beta E_x^{(\pm)2}E_y^{(\pm)*} + 2\beta E_x^{(\pm)}E_x^{(\mp)}E_y^{(\mp)*}=0. \tag{5}$$

Note that the coupled-mode approach applied for temporal solitons in fiber Bragg gratings results in an equivalent set of equations. In the fiber case, z should be interpreted as local time and x as a coordinate along the fiber. Though experimental relevance of the existence of vector gap solitons in fibers has been outlined in recent work [13], we are not aware of any theoretical studies.

III. FAMILIES OF BRAGG SOLITONS

We focus below on the properties of spatial Bragg solitons propagating parallel to the z axis. Practical excitation of these structures should require use of a strongly diffracting initial beam profile with suitable wavelength, which can provide sufficiently strong scattering from the grating. Equivalently, one can use two input beams propagating at an angle to z axis, see Fig. 1. The latter scheme is equivalent to the one suggested in Ref. [14] for excitation of parametric Bragg solitons. From a mathematical point of view, propagation of a spatial soliton is equivalent to the zero velocity solitons in Bragg fibers [14]. Selective modeling of Eqs. (4) and (5) indicates that introducing nonzero velocity through the substitution $(x,z)\rightarrow(x-vz,z)$, does not generally lead to dynamics qualitatively different from those described below.

We seek solitary solutions of Eqs. (4) and (5) in the form

$$E_{x,y}^{(\pm)}=A_{x,y}^{(\pm)}(x,q)e^{iqz}. \tag{6}$$

Parametrization by q naturally follows from the single phase invariance of the Eq. (1),

$$(E_r,E_l)\rightarrow(E_re^{i\phi},E_le^{i\phi}), \tag{7}$$

where ϕ is an arbitrary phase. Numerically solving the resulting set of ordinary differential equations for $A_{x,y}^{(\pm)}$, we have been able to identify four soliton families. First, there are two linearly polarized solitons: (i) $A_x^{(\pm)}=0$, $A_y^{(\pm)}\neq 0$ and (ii) $A_x^{(\pm)}\neq 0$, $A_y^{(\pm)}=0$. The stationary profiles of the linearly polarized solitons obviously coincide with those known in closed analytical form for the scalar problem [2]. The two families of the linearly polarized solitons are straightforwardly transformed one into another using $A_x^{(\pm)}(q,x)=A_y^{(\pm)}(q+\delta,x)$. Second, there are two families of elliptically polarized solitons: (iii) $A_x^{(\pm)}\neq 0$, $A_y^{(\pm)}\neq 0$ and (iv) the family obtained from the third by inverting the sign of either x- or y-polarized components (which corresponds to the opposite direction of the rotation of the polarization vector).

A bifurcation diagram showing dependence of the total soliton power P ($\partial_z P=0$),

$$P=\int dx(|E_x^+|^2+|E_x^-|^2+|E_y^+|^2+|E_y^-|^2) \tag{8}$$

vs δ for all the above mentioned Bragg solitons, and corresponding examples of the soliton transverse profiles are shown in Figs. 2 and 3.

The necessary conditions for existence of the Bragg solitons can be found from analysis of the decay of the soliton tails. Linearly polarized solitons can exist if $|q|<1$ (x polarization) or $|q+\delta|<1$ (y polarization). The power of the x-polarized soliton is obviously δ independent, see Fig. 2. The peak intensity of the linearly polarized solitons goes down when q approaches the lower boundary of the forbidden gap from above, i.e., $q,(q+\delta)\rightarrow -1$, providing that nonlinearity is defocusing, i.e., $\alpha+\beta<0$. When the nonlinearity has the right sign, a relatively small intensity is enough to push the effective frequency down into the ''valence'' band. In contrast, if $q,(q+\delta)\rightarrow 1$, i.e., when q approaches the upper boundary of the forbidden gap, the peak intensity of the soliton should be very high to produce a nonlinear shift of the wave number large enough to bring it into the ''valence'' band. A focusing nonlinearity pushes the effective wave number up towards the ''conduction'' band, so revers-

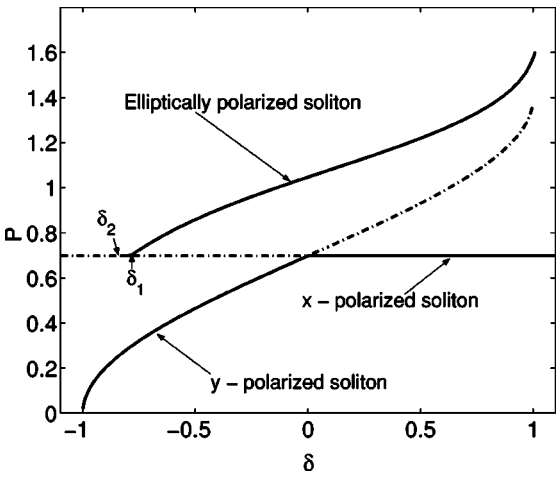

FIG. 2. Dependences of the soliton power on the anisotropy parameter δ for linearly and elliptically polarized solitons. Dashed lines show regions of polarization instability. Parameters are $q=0$, $\alpha=-2$, $\beta=-1$.

ing the picture just described. Elliptically polarized solitons exist if $\max(|q|,|q+\delta|)<1$, i.e., inside the range of wave numbers, for which the propagation of linear waves is forbidden for both polarizations. An elliptical soliton family detaches from the linear one at some critical value of $\delta=\delta_1$ and it ceases to exist at $q+\delta\to 1$, when the band gap boundary for *y* polarization is achieved, see Fig. 2.

Because of the birefringence, the decay rate of the soliton tails is different for *x* and *y* polarizations. For example, if $|q|$ is closer to 1 than $|q+\delta|$, the polarization ellipse at the soliton tail is elongated along the *x* axis, and along *y* axis if vice versa. In the vicinity of the point where the elliptical soliton splits from the *x*-polarized one, i.e., at $\delta=\delta_1$, see Fig. 2, the former has a core with nearly *x* polarization and tails with nearly *y* polarization, i.e., the polarization state rotates by approximately 90°, as position varies from the soliton core to its periphery, see Fig. 4.

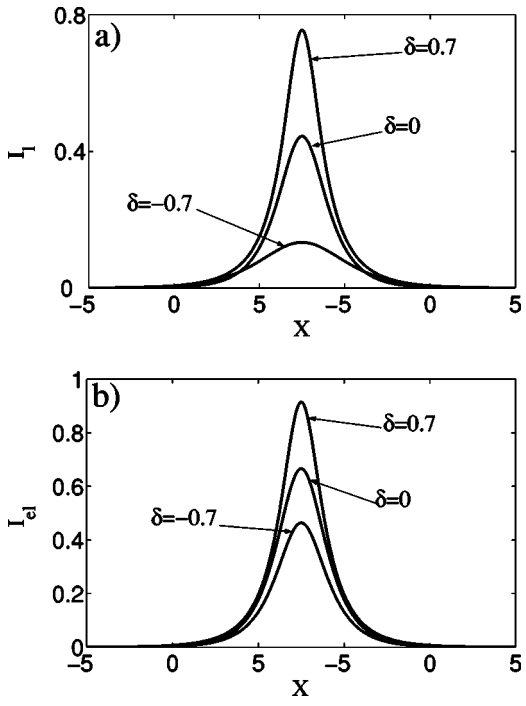

FIG. 3. Intensity distributions for the *y*-polarized soliton (a), $I_y=|A_y^+|^2+|A_y^-|^2$, and for the elliptical soliton (b), $I_{el}=|A_x^+|^2+|A_x^-|^2+|A_y^+|^2+|A_y^-|^2$, for different values of δ. Parameters as in Fig. 1.

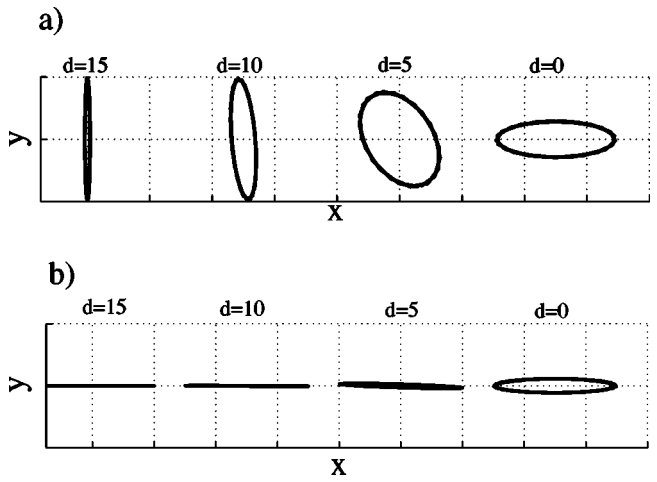

FIG. 4. Polarization state at distance *d* from the center of the elliptically polarized soliton for different parameters: (a) $q=0$, $\delta=-0.7$, (b) $q=0.9$, $\delta=-1.46$.

Note that Eqs. (4) and (5) remain unchanged after substitution

$$(\delta,\alpha,\beta,E_{x,y}^{(+)},E_{x,y}^{(-)})\to(-\delta,-\alpha,-\beta,E_{x,y}^{(+)*},-E_{x,y}^{(-)*}).$$

Therefore, without the loss of generality we can fix the sign of α and β to negative. Then changing sign of δ we will effectively study both focusing $(\alpha,\beta>0)$ and defocusing $(\alpha,\beta<0)$ nonlinearities. In all subsequent calculations, we fix $\alpha=-2$, $\beta=-1$, which corresponds to the defocusing electronic nonlinearity.

IV. STABILITY ANALYSIS

After establishing the existence of the soliton families in the problem, we now turn our attention to their stability analysis.

A. Analytics

Though full stability analysis is possible only by the means of numerical methods, some results on stability of the *x*-polarized solitons can be derived analytically. For this purpose it is easier to use governing equations in the form (1). We proceed by linearizing Eq. (1) through the substitution

$$E_{r,l}=[A_{r,l}(x)+U_{r,l}(x,z)+iW_{r,l}(x,z)]e^{iqz}, \qquad (9)$$

where $A_{r,l}(x)$ are real functions characterizing transverse profiles of the soliton components in circular basis and $U_{r,l}$, $W_{r,l}$ are small real perturbations. After separation of real and imaginary parts, in the first perturbation order, we derive a system of linear equations:

$$(\hat{\mathcal{T}}-\delta\hat{\tau})\vec{U}=-\partial_z\vec{W}, \tag{10}$$

$$(\hat{\mathcal{P}}-\delta\hat{\tau})\vec{W}=\partial_z\vec{U},$$

where $\vec{U}=(U_r,U_l)^T$, $\vec{W}=(W_r,W_l)^T$,

$$\hat{\tau}=\frac{1}{2}\begin{pmatrix}1 & -1\\ -1 & 1\end{pmatrix}, \tag{11}$$

$\hat{\mathcal{P}}$ are $\hat{\mathcal{T}}$ self-adjoint operators:

$$\hat{\mathcal{P}}=\begin{pmatrix}\hat{D}-\alpha A_r^2-(\alpha+2\beta)A_l^2 & 0\\ 0 & \hat{D}-\alpha A_l^2-(\alpha+2\beta)A_r^2\end{pmatrix}, \tag{12}$$

$$\hat{\mathcal{T}}=\begin{pmatrix}\hat{D}-3\alpha A_r^2-(\alpha+2\beta)A_l^2 & -2(\alpha+2\beta)A_lA_r\\ -2(\alpha+2\beta)A_lA_r & \hat{D}-3\alpha A_l^2-(\alpha+2\beta)A_r^2\end{pmatrix}, \tag{13}$$

and $\hat{D}=-\partial_x^2+\kappa-f(x)$. Assuming exponential evolution of the perturbations, i.e., $\vec{U}(x,z)=\vec{u}(x)e^{\lambda z}+\vec{u}^*(x)e^{\lambda^* z}$, $\vec{W}(x,z)=\vec{w}(x)e^{\lambda z}+\vec{w}^*(x)e^{\lambda^* z}$, Eq. (10) are straightforwardly reduced to a linear eigenvalue problem.

In the special case $\delta=0$, Eq. (1) acquire an additional symmetry group

$$(E_r,E_l)\to(E_re^{i\psi},E_le^{-i\psi}), \tag{14}$$

where ψ is a second arbitrary phase. Linearly and elliptically polarized solitons become, in this case, members of a single soliton family. This is because the second phase invariance implies existence of a second family parameter Δ and solitons can be sought in the form

$$E_r=A_{r0}(x)e^{iqz+i\Delta z+i\phi+i\psi},\quad E_l=A_{l0}(x)e^{iqz-i\Delta z+i\phi-i\psi}. \tag{15}$$

This new parametrization opens up a possibility to develop an asymptotic theory of polarization instability of linearly polarized solitons for small values of δ. The case of x-polarized solution $A_r=A_l=A$ provides a particularly transparent example, because in this case the function A does not itself depend on δ, see Eq. (1).

For $\delta=0$ the infinitesimal symmetry transformations (14) applied to the x-polarized soliton generates a Goldstone or neutral soliton eigenmode $\vec{w}=\vec{w}_\psi=(A,-A)^T$, $\vec{u}=0$ having zero eigenvalue, i.e., $\lambda=0$. The zero eigenvalues corresponding to the Goldstone modes in Hamiltonian systems are always evenly degenerate, see, e.g., Ref. [15]. In our case double degeneracy is realized and therefore, when the symmetry (14) is broken by nonzero values of δ, either two imaginary or two real eigenvalues with opposite signs appear in the soliton spectrum, generating instability in the latter case. To work out conditions for this instability, we transform Eq. (10) to the form

$$\hat{\mathcal{T}}\hat{\mathcal{P}}\vec{w}=(-\lambda^2+\delta\hat{\mathcal{T}}\hat{\tau}+\delta\hat{\mathcal{T}}\hat{\tau}+\delta^2\hat{\tau}^2)\vec{w}. \tag{16}$$

We assume that $|\lambda|^2\sim|\delta|$ and search for solutions of Eq. (16) in the form

$$\vec{w}=\vec{w}_\psi+\vec{w}_1+O(|\delta|^2), \tag{17}$$

where the components of $\vec{w}_1$ are of order $|\delta|$. Then solvability conditions in the first order require orthogonality of the vector $\vec{R}=\lambda^2\vec{w}_\psi+\delta\hat{\mathcal{T}}\hat{\tau}\vec{w}_\psi$ to the null space of the operator adjoint to $\hat{\mathcal{T}}\hat{\mathcal{P}}$, i.e., $\hat{\mathcal{P}}\hat{\mathcal{T}}$. The null space of the latter is spanned by the two vectors $\vec{u}_q=\partial_q(A,A)^T$ and $\vec{u}_\Delta=[\partial_\Delta(A_{r0},A_{l0})]_{\Delta=0}^T$. The verification of $\hat{\mathcal{P}}\hat{\mathcal{T}}\vec{u}_\Delta=0$ requires the linearization procedure to be done for $\delta=0$ in the vicinity of the two-parameter soliton family (15). This reveals explicit dependence of $\hat{\mathcal{P}}$ and $\hat{\mathcal{T}}$ on Δ, which can, in its turn, be used to check that $\hat{\mathcal{P}}(\hat{\mathcal{T}}\vec{u}_\Delta)=-\hat{\mathcal{P}}\vec{w}_\psi=0$.

The orthogonality of $\vec{R}$ to $\vec{u}_q$ is satisfied unconditionally, while orthogonality to $\vec{u}_\Delta$ requires $\lambda^2\langle\vec{w}_\psi|\vec{u}_\Delta\rangle+\delta\langle\hat{\mathcal{T}}\hat{\tau}\vec{w}_\psi|\vec{u}_\Delta\rangle=\lambda^2\langle\vec{w}_\psi|\vec{u}_\Delta\rangle-\delta\langle\hat{\tau}\vec{w}_\psi|\vec{w}_\psi\rangle=0$, which gives

$$\lambda^2=\frac{-4\delta\int_{-\infty}^{+\infty}dxA^2}{\left[\partial_\Delta\int_{-\infty}^{+\infty}dx(A_{r0}^2-A_{l0}^2)\right]_{\Delta=0}}. \tag{18}$$

Despite the fact that integrals in Eq. (18) can be calculated only numerically, this expression gives a clear indication that a change in sign of δ results in instability of the soliton. As it can be seen from the structure of the excited eigenmode, the perturbations growing as a result of the instability have y polarization because the corresponding left- and right-polarized components are equal in magnitude, but have opposite signs. To verify our analytical results, and further develop our understanding of polarization instabilities of Bragg solitons, we describe below an extensive numerical study of the polarization dynamics of gap solitons.

B. Numerical results

All our numerical results are obtained within the approximation of slowly varying amplitudes and therefore from now on we make full use of Eqs. (4) and (5). Their linearization near the soliton solution $A_x^{(\pm)}\neq0$, $A_y^{(\pm)}=0$ leads to two independent eigenvalue problems for the operators $\hat{\mathcal{L}}_{x,y}$, see the Appendix. Eigenstates of $\hat{\mathcal{L}}_x$ determine the evolution of

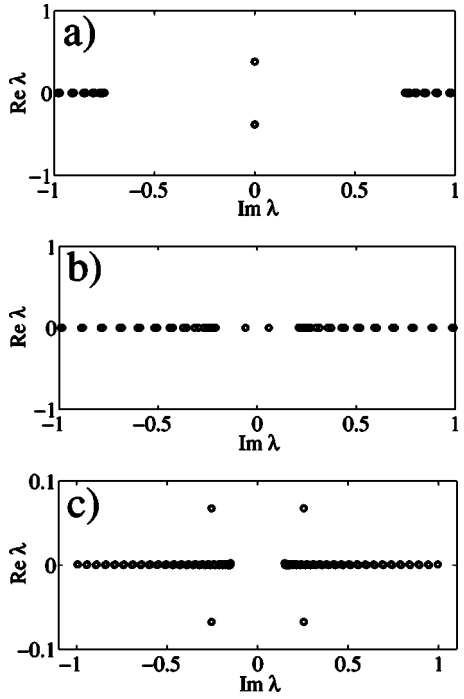

FIG. 5. Spectra of $\hat{\mathcal{L}}_y$ for different values of δ: (a) $\delta=-0.25$, (b) $\delta=-0.8$, (c) $\delta=-0.85$. Other parameters as in Fig. 1.

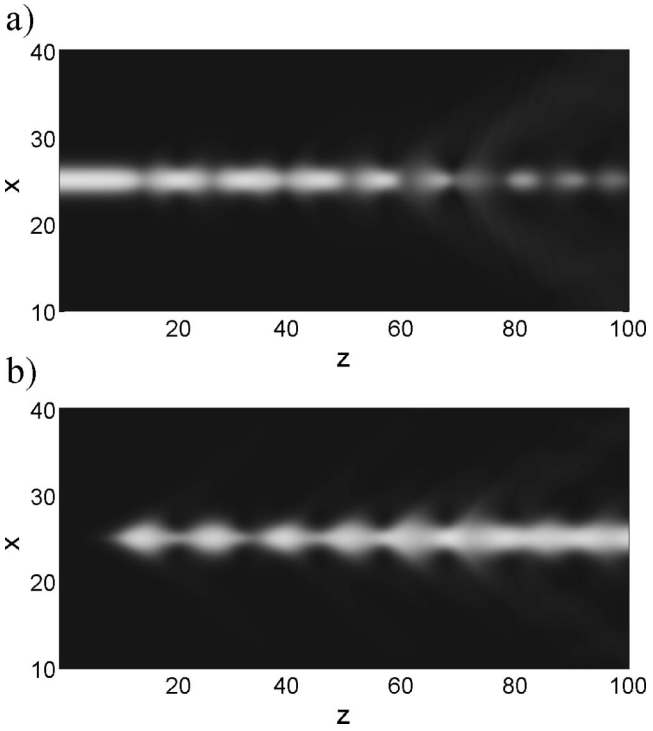

FIG. 7. x-z plots showing evolution of $|E_x^{(+)}|^2+|E_x^{(-)}|^2$ (a) and $|E_y^{(+)}|^2+|E_y^{(-)}|^2$ (b), when Eqs. (4) and (5) are initialized with an x-polarized soliton perturbed by noise. The parameters are $q=0$ and $\delta=-0.25$.

x-polarized perturbations, which, in the circular basis, have identical left and right components. The spectral properties of $\hat{\mathcal{L}}_x$ have been studied in detail in several previous papers [8], and it has been found that under the certain conditions a quadruplet of complex eigenvalues close to the continuum part of the spectrum generates a *scalar* instability of gap solitons.

The dynamics of y-polarized perturbations is governed by the eigenstates of the operator $\hat{\mathcal{L}}_y$, which is δ dependent. The spectrum of $\hat{\mathcal{L}}_y$ has a doubly degenerate zero eigenvalue at $\delta=0$, which in the circular basis corresponds to the neutral eigenmode $\vec{w}_\psi$. Numerically tracing a deviation of these eigenvalues from zero, we have found that instability, i.e., a pair of real eigenvalues, appears for $\delta<0$, see Fig. 5 and Eq. (18). Excellent agreement between the numerical and the analytical results for small absolute values of δ can be seen in Fig. 6. The high-density regions of the spectrum seen in Fig. 5 correspond to the continuum, which is divided in two parts by the central gap, $|q+\delta|-1<\mathrm{Im}\lambda<1-|q+\delta|$, where the stable eigenmodes belonging to the discrete part of the spectrum can be found, see Fig. 5(b).

The direct numerical simulation of Eqs. (4) and (5), with initial conditions taken as an x-polarized soliton plus seeded noise of both polarizations, shows an initial growth rate of the y- component within 5% of the value found from the spectral problem. After the transient regime the instability generally leads to the formation of an oscillatory solitonic state, see Fig. 7, which is close to the elliptical soliton. Note that stability analysis of the latter lies outside our present scope. Radiation losses have been found minimal during development of the instability, which agrees well with good localization of the unstable eigenvector within the region of localization of the soliton itself, see Fig. 8. Thus the polar-

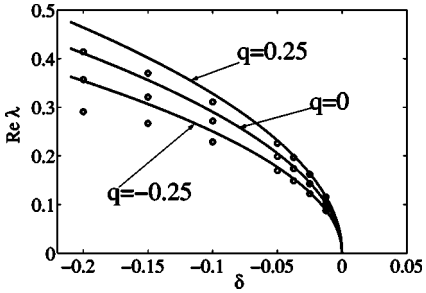

FIG. 6. Comparison of numerical results (circles) for the polarization instability growth rate with the analytical predictions, [Eq. (18)], (solid lines). Parameters as in Fig. 1.

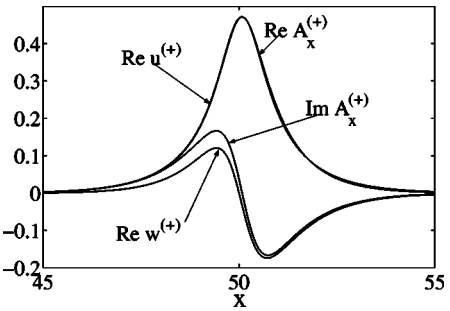

FIG. 8. Components of the eigenvector generating polarization instability. The corresponding spectrum is shown in Fig. 5(a).

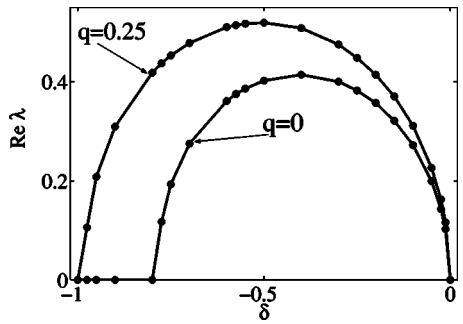

FIG. 9. Growth rate of the waveguide-type instability vs δ. The corresponding spectrum is shown in Fig. 5(a).

ization instability found for small negative δ can be interpreted as parametric excitation of guided *y*-polarized waves in the waveguide formed by the *x*-polarized soliton, i.e., *waveguide* instability.

With further increase of $|\delta|$ the instability growth rate approaches its maximum, then it starts to decrease in value and finally the positive and negative eigenvalues fuse at zero for $\delta=\delta_1$, see Fig. 9. This appears to be exactly the point where the elliptic soliton family detaches from the *x*-polarized one. For larger $|\delta|$ the eigenvalues, we are tracing, quickly move along the imaginary axis, see Fig. 5(b), towards the edge of the continuum spectrum. For some $\delta=\delta_2$, as a result of collision with eigenvalues close to the edge of the continuum spectrum, four complex eigenvalues appear in the soliton spectrum, see Fig. 5(c). Two of these have positive real parts thereby generating Hamiltonian-Hopf instability of the *x*-polarized soliton. With further increase of $|\delta|$ the instability growth rate decreases slowly. It seems that its existence region is not bounded from the left, see Fig. 10.

The eigenvectors corresponding to the latter instability are weakly localized relatively to the soliton itself and have oscillatory tails, see Fig. 11. The direct numerical simulation reveals that energy flow from the *x* to the *y* component is followed by substantial radiation of energy out of the effective waveguide created by the soliton, see Fig. 12. This could be expected from the form of the eigenvectors. Thus this

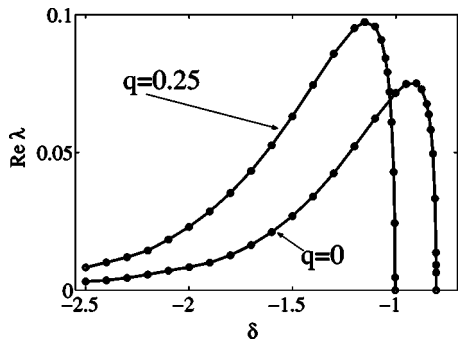

FIG. 10. Growth rate of the radiative-type instability vs δ. The corresponding spectrum is shown in Fig. 5(c).

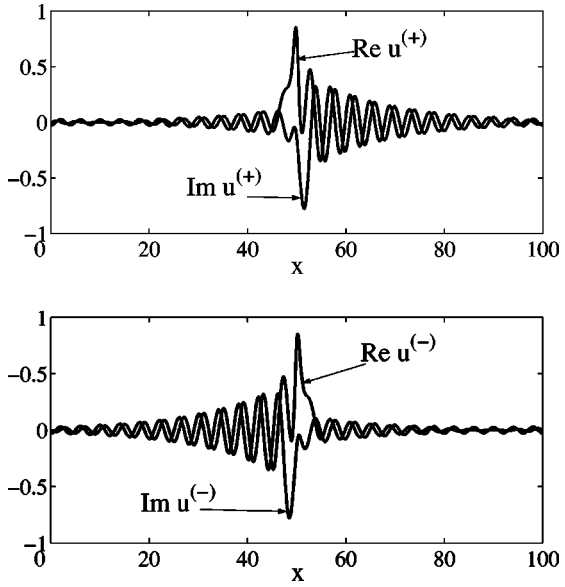

FIG. 11. Components of the eigenvector generating radiative instability. Parameters are $\delta=-1.2$, $q=0$.

type of the polarization instability can be naturally referred to as the *radiative* instability. The amount of energy emitted into nonsolitonic forms decreases with propagation, finally leading to the formation of a solitonlike structure with elliptical polarization state, similarly to what happens as a result of the waveguide-type instability for small negative δ. The characteristic angle of radiation increases, from being small

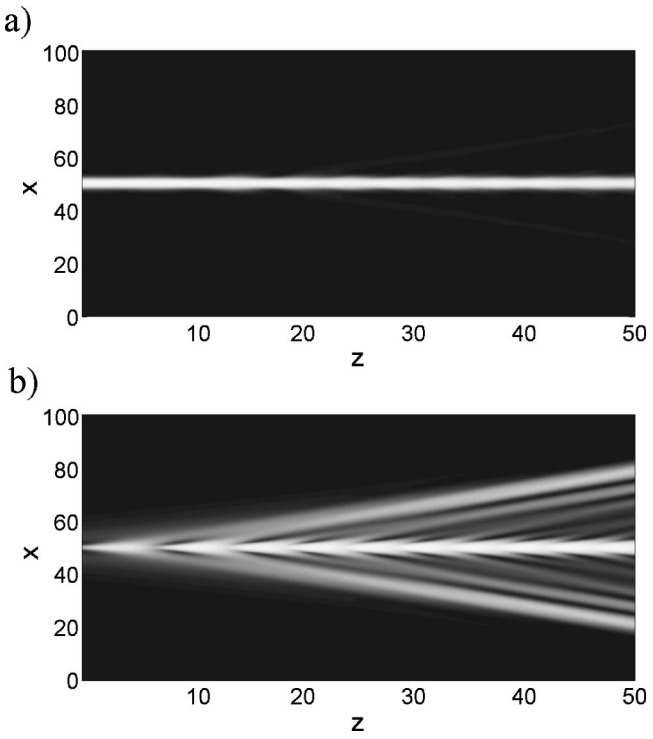

FIG. 12. *x*-*z* plots showing evolution of $|E_x^{(+)}|^2+|E_x^{(-)}|^2$ (a) and $|E_y^{(+)}|^2+|E_y^{(-)}|^2$ (b), when Eqs. (4) and (5) are initialized with an *x*-polarized soliton perturbed by noise. Parameters are $q=0$, $\delta=-0.85$.

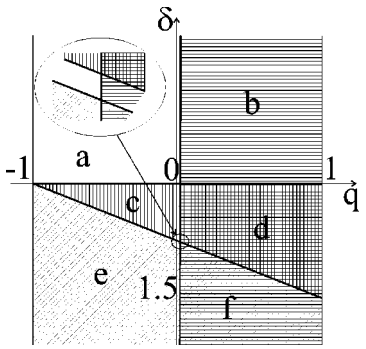

FIG. 13. Diagram showing the regions of polarization and scalar instabilities. Region *"a"* is the region, where an *x*-polarized soliton is stable. Region *"b"* is the region where it is unstable due to scalar instability. Region *"c"* is the region where it is unstable to the waveguide-type polarization instability. In region *"d"* both scalar and waveguide polarization instabilities are present. Region *"e"* is the domain of radiative polarization instability, *"f"* is the region of coexistence of the scalar and polarization radiative instabilities. The sloping line separating regions of different stabilities is in fact two lines that begin at $\delta=0$, $q=-1$ and go very close to each other. The inset shows a narrow region of stability between these two lines.

for δ close to δ_2 to being close to $\pi/2$, when $\delta\to-\infty$. A qualitative explanation for this dependence can be based on the assumption that one of the conditions for the radiative instability should be in synchronism between the soliton and some plane wave with wave vector lying outside the forbidden band. Taking a *y*-polarized plane wave in the form $e^{iq_z z+iq_x x}$, we find a dispersion relation in the form $(\delta-q_z)^2-q_x^2=1$. Synchronism requires $q_z=q$, where q is the shift of the soliton wave number. This gives an estimate for the characteristic angle of radiation: ϕ, $\phi\sim\pm\arctan(\sqrt{(\delta-q)^2-1}/q)$. Though this expression qualitatively reproduces the numerically observed dependence of ϕ on δ, one should bear in mind that the dispersive properties of waves emitted by a soliton are of course different from those of plane waves, which limits this and other possible applications of the synchronism condition.

The polarization instabilities found here can usually compete with the scalar instabilities reported in Ref. [8]. An important observation in this context is that the scalar instability exists only for $q>0$ [8], i.e., in the top half of the forbidden band, while polarization instability can be present for any q and is controlled by the sign of δ. The unstable regions in the (q,δ) plane are shown in Fig. 13. If both instabilities are present, either can dominate depending on the values of the parameters.

V. SUMMARY

We have studied existence of linearly and elliptically polarized spatial Bragg solitons propagating in one-dimensional Kerr media with periodic modulation of the refractive index transverse to the propagation direction. Polarization instabilities of the linearly polarized solitons have been analyzed in detail and two qualitatively distinct instability scenarios have been found. One instability is of the waveguide type. It appears for arbitrarily small birefringence and leads to energy transfer from the linearly polarized soliton state to the orthogonally polarized waves that are well confined inside the soliton-induced waveguide. Another polarization instability is of the radiative type. The soliton emits energy through the excitation of orthogonally polarized waves that propagate at an angle to the soliton propagation direction, thereby leading to the substantial energy transfer to nonlocalized nonsolitonic forms. This instability is observed for relatively large birefringence. Both polarization instabilities happen for solitons polarized along the axis with higher refractive index, providing the nonlinearity is self-defocusing, i.e., these are slow wave instabilities. If the nonlinearity is focusing, the picture reverses, and the instabilities become fast wave instabilities, similar to the polarization instabilities known for Schrödinger-type solitons [4]. Note that the general perturbation theory of polarization instabilities in the limit of small birefringence, developed above, can also be applied for Schrödinger solitons.

ACKNOWLEDGMENTS

Support from the UK EPSRC through Grant Nos. GR/N19830 and GR/R 74918 is acknowledged.

APPENDIX

We linearize coupled-mode approach Eqs. (4) and (5) near the *x*-polarized soliton, $E_x^{(\pm)}=A_x^{(\pm)}\exp(iqz)$, $E_y^{(\pm)}=0$, through the substitution $E_x^{(\pm)}=(A^{(\pm)}+e_x^{(\pm)})\exp(iqz)$, $E_y^{(\pm)}=e_y^{(\pm)}\exp(iqz)$, where $e_{x,y}^{(\pm)}$ are small corrections. For the sake of brevity, we omit subscript x in $A_x^{(\pm)}$ throughout this appendix.

Linearization leads to two independent systems for $e_x^{(\pm)}$ and $e_y^{(\pm)}$. Splitting real and imaginary parts through the substitutions $e_j^{(\pm)}=v_j^{(\pm)}+i\,\nu_j^{(\pm)}$, where $j=x,y$, we find

$$-\partial_z v_j^{(\pm)}=[\pm\partial_x+\mathrm{Im}(q_j^{(\pm)})]v_j^{(\pm)}+[p_j-\mathrm{Re}(q_j^{(\pm)})]\nu_j^{(\pm)}+\mathrm{Im}(r_j^{(\pm)}+s_j)v_j^{(\mp)}+\mathrm{Re}(r_j^{(\pm)}-s_j)\nu_j^{(\mp)}, \quad \text{(A1)}$$

$$-\partial_z \nu_j^{(\pm)}=[\pm\partial_x-\mathrm{Im}(q_j^{(\pm)})]\nu_j^{(\pm)}-[p_j+\mathrm{Re}(q_j^{(\pm)})]v_j^{(\pm)}+\mathrm{Im}(r_j^{(\pm)}-s_j)\nu_j^{(\mp)}-\mathrm{Re}(r_j^{(\pm)}+s_j)v_j^{(\mp)}, \quad \text{(A2)}$$

where $p_x=q+2(\alpha+\beta)(|A^{(+)}|^2+|A^{(-)}|^2)$, $q_x^{(\pm)}=(\alpha+\beta)A^{(\pm)2}$, $r_x^{(\pm)}=2(\alpha+\beta)A^{(\pm)}A^{(\mp)*}$, $s_x=2(\alpha+\beta)A^{(+)}A^{(-)}$, $p_y=q+\delta+\alpha(|A^{(+)}|^2+|A^{(-)}|^2)$, $q_y^{(\pm)}=\beta A^{(\pm)2}$, $r_y^{(\pm)}=\alpha A^{(\pm)}A^{(\mp)*}$, and $s_y=2\beta A^{(+)}A^{(-)}$.

Now we can write the equation governing the dynamics of a small correction in the form

$$\partial_z\vec{v}_j=\hat{\mathcal{L}}_j\vec{v}_j, \quad j=x,y, \quad \text{(A3)}$$

where $\vec{v}_j=(v_j^{(+)},\nu_j^{(+)},v_j^{(-)},\nu_j^{(-)})^T$ and $\hat{\mathcal{L}}_j$ are the linear operators

$$\hat{\mathcal{L}}_j = -\begin{pmatrix} \partial_x + \mathrm{Im}(q_j^{(+)}) & p_j - \mathrm{Re}(q_j^{(+)}) & \mathrm{Im}(r_j^{(+)} + s_j) & \mathrm{Re}(r_j^{(+)} - s_j) \\ -p_j + \mathrm{Re}(q_j^{(+)}) & \partial_x - \mathrm{Im}(q_j^{(+)}) & -\mathrm{Re}(r_j^{(+)} + s_j) & \mathrm{Im}(r_j^{(+)} - s_j) \\ \mathrm{Im}(r_j^{(-)} + s_j) & \mathrm{Re}(r_j^{(-)} - s_j) & -\partial_x + \mathrm{Im}(q_j^{(-)}) & p_j - \mathrm{Re}(q_j^{(-)}) \\ -\mathrm{Re}(r_j^{(-)} + s_j) & \mathrm{Im}(r_j^{(-)} - s_j) & -p_j - \mathrm{Re}(q_j^{(-)}) & -\partial_x - \mathrm{Im}(q_j^{(-)}) \end{pmatrix}. \tag{A4}$$

Equations (A3) are reduced to eigenvalue problems through the substitutions $\vec{\nu}^{(\pm)}(x,z) = \vec{\omega}^{(\pm)}(x)e^{\lambda z} + \vec{\omega}^{(\pm)*}(x)e^{-\lambda z}$ and $\vec{\nu}^{(\pm)}(x,z) = \vec{\varpi}^{(\pm)}(x)e^{\lambda z} + \vec{\varpi}^{(\pm)*}(x)e^{-\lambda z}$. The spectral properties of the operators $\hat{\mathcal{L}}_{x,y}$ define the stability of the soliton and are discussed in the main sections of the paper.

[1] D.L. Miles, *Nonlinear Optics* (Springer, Berlin, 1998), Chap. 7, and references therein.

[2] B.J. Eggleton, C.M. de Sterke, and R.E. Slusher, J. Opt. Soc. Am. B **16**, 587 (1999), and references therein.

[3] *Confined Electrons and Photons: New Physics and Applications*, edited by E. Burstein and C. Weisbuch (Plenum Press, New York, 1995).

[4] E.A. Ostrovskaya, N.N. Akhmediev, G.I. Stegeman, J.U. Kang, and J.S. Aitchison, J. Opt. Soc. Am. B **14**, 880 (1997).

[5] L. Friedrich, R. Malendevich, G.I. Stegeman, J.M. Soto-Crespo, N.N. Akhmediev, and J.S. Aitchison, Opt. Commun. **186**, 335 (2000).

[6] D.C. Hutchings and J.M. Arnold, J. Opt. Soc. Am. B **16**, 513 (1999).

[7] D. Mihalache, D. Mazilu, and L. Torner, Phys. Rev. Lett. **81**, 4353 (1998).

[8] I.V. Barashenkov, D.E. Pelinovsky, and E.V. Zemlyanaya, Phys. Rev. Lett. **80**, 5117 (1998).

[9] A. De Rossi, C. Conti, and S. Trillo, Phys. Rev. Lett. **81**, 85 (1998).

[10] J. Schöllmann and A.P. Mayer, Phys. Rev. E **61**, 5830 (2000).

[11] D.V. Skryabin and W.J. Firth, Phys. Rev. E **60**, 1019 (1999).

[12] R.W. Boyd, *Nonlinear Optics* (Academic Press, Boston, 1992).

[13] R.E. Slusher, S. Spälter, B.J. Eggleton, S. Pereira, and J.E. Sipe, Opt. Lett. **25**, 749 (2000).

[14] C. Conti, G. Assanto, and S. Trillo, Opt. Lett. **22**, 1350 (1997).

[15] D.V. Skryabin, Physica D **139**, 186 (2000).